



HAL
open science

Analytical modeling of one-dimensional resonant asymmetric and reciprocal acoustic structures as Willis materials

Jean-Philippe Groby, M Malléjac, Aurélien Merkel, Vicente Romero-García, Vincent Tournat, Daniel Torrent, Jensen Li

► To cite this version:

Jean-Philippe Groby, M Malléjac, Aurélien Merkel, Vicente Romero-García, Vincent Tournat, et al.. Analytical modeling of one-dimensional resonant asymmetric and reciprocal acoustic structures as Willis materials. *New Journal of Physics*, 2021, 23 (5), pp.053020. 10.1088/1367-2630/abfab0 . hal-03436149

HAL Id: hal-03436149

<https://hal.science/hal-03436149>

Submitted on 23 Nov 2021

HAL is a multi-disciplinary open access archive for the deposit and dissemination of scientific research documents, whether they are published or not. The documents may come from teaching and research institutions in France or abroad, or from public or private research centers.

L'archive ouverte pluridisciplinaire **HAL**, est destinée au dépôt et à la diffusion de documents scientifiques de niveau recherche, publiés ou non, émanant des établissements d'enseignement et de recherche français ou étrangers, des laboratoires publics ou privés.

Analytical modeling of one-dimensional resonant asymmetric and reciprocal acoustic structures as Willis materials

Jean-Philippe Groby¹, Matthieu Malledjac¹, Aurélien Merkel²,
Vicente Romero-García¹, Vincent Tournat¹, Daniel Torrent³,
and Jensen Li⁴

¹Laboratoire d'Acoustique de l'Université du Mans (LAUM), UMR CNRS 6613,
Institut d'Acoustique - Graduate School (IA-GS), CNRS, Le Mans Université, France

²Institut Jean Lamour and University of Lorraine in Nancy, France

³GROC, UJI, Institut de Noves Tecnologies de la Imatge (INIT), Universitat Jaume I, 12071 Castelló, Spain

⁴Department of Physics, The Hong Kong University of Science and Technology, Clear Water Bay, Hong Kong, China

August 2017

Abstract. As building blocks of acoustic metamaterials, resonant scatterers have demonstrated their ability to modulate the effective fluid parameters, which subsequently possess extreme properties such as negative bulk modulus or negative mass density. Promising applications have been shown such as extraordinary absorption, focusing, and abnormal refraction for instance. However, acoustic waves can be further controlled in Willis materials by harnessing the coupling parameters. In this work, we derive the closed forms of the effective parameters from the transfer matrix in three asymmetric and reciprocal one-dimensional resonant configurations and exhibit the differences in terms of coupling coefficients. The way in which Willis coupling occurs in spatially asymmetric unit cells is highlighted. In addition, the analysis shows the absence of odd Willis coupling for reciprocal configurations. These effective parameters are validated against experimental and numerical results in the three configurations. This article paves the way of a novel physical understanding and engineering use of Willis acoustic materials.

1. Introduction

Since the seminal work of Willis in the 80's [1], the eponymous materials have received an increasing attention, because of their analogy with bi-isotropic electromagnetic metamaterials [2]. The Willis coupling parameters couple the potential and kinetic energy in the acoustic conservation relations, therefore enhancing the ability to control waves in metamaterials compared to other materials that do not exhibit such coupling. These parameters have thus been employed to design \mathcal{PT} symmetric [3], wave front shaping [4, 5], or non-reciprocal [6] systems. Willis coupling arises from chiral

inhomogeneities [7], asymmetric inhomogeneities, nonlocal effects, and nonreciprocal biases [8]. Although most of the works to date have focused on the experimental evidence [4, 9, 10], physical origins [11], calculation [12, 13, 14], and enhancement [15] of Willis coupling, only a few have focused on deriving a closed form of these parameters. The present article aims at filling this gap and therefore at easing its physical understanding and engineering use. Effectively, it turns out that various systems rely on asymmetric meta-atoms for perfect absorption in transmission problem [16], non-Hermiticity of the acoustic waves [17], \mathcal{PT} symmetry [18], or more generally most of the double negative one-dimensional devices [19, 20, 11].

We focus on three resonant, asymmetric, and reciprocal one-dimensional unit cells and derive closed forms of the corresponding Willis coupling parameters, exhibiting different forms depending on the nature of the asymmetry. By analyzing these Willis parameters, we show that Willis coupling in resonant systems arises from first order Taylor expansion originating differently from multilayer systems [21, 13, 22] and exhibit the dipolar feature of the coupling via arm terms. In addition, the reciprocity condition directly provides even coupling and vanishing odd coupling [11], thus inducing doubt on the existence of odd coupling in one-dimensional reciprocal acoustic systems. While even Willis coupling parameters appear with opposite sign in the propagation matrix, odd Willis coupling appear with identical sign in the propagation matrix for reciprocal structures.

The article is organized as follows. The general procedure for the derivation of the effective parameters is detailed in Section 2. It relies on the Padé's approximation of the total transfer matrix, which links the state vectors at both sides of a unit cell. The procedure is applied in Section 3 to three different resonant asymmetric and reciprocal one-dimensional unit cells. While the first two unit cells are composed of detuned resonators either in parallel or in series of a duct, the third one combines resonators in parallel and in series in the duct, see Fig. 1. Two of these unit cells have already been studied as Willis materials [11, 9], but the closed forms of the coupling parameters have not been provided. The derived forms clearly unveil dipolar feature of Willis coupling, as well as the differences between resonant and non-resonant asymmetries and nature of the resonant asymmetry. The effective parameters are validated against experimental and numerical (derived from [13]) results for each unit cell in Section 4. The order of Taylor expansion required to correctly model an asymmetric resonant unit cell is questioned. Finally, concluding remarks and perspectives are provided. Additional information are also given in appendices.

2. Derivation of the Willis coupling parameters

We consider a one-dimensional asymmetric and reciprocal material composed of the periodic repetition of a unit cell of length d . The pressure and particle velocity (alternatively the flow in a duct) form a state vector $\mathbf{W}^T = \langle p, \mathcal{V} \rangle$, where T is the transpose operator. This state vector satisfies the following matrix equation which

directly arises from the mass conservation and constitutive law:

$$\frac{d}{dx}\mathbf{W} = \mathbf{A}\mathbf{W}. \quad (1)$$

Assuming an implicit time dependence $e^{-i\omega t}$, the matrix \mathbf{A} reads as

$$\mathbf{A} = i\omega \begin{bmatrix} \chi & \rho \\ 1/K & -\chi \end{bmatrix}, \quad (2)$$

for Willis type materials, where ρ , K and χ are respectively the density, bulk modulus and Willis coupling parameter. Please note that a usual isotropic and symmetric effective fluid implies $\chi = 0$. The state vectors at both sides of the unit cell, $\mathbf{W}(d)$ and $\mathbf{W}(0)$, are thus linked by

$$\mathbf{W}(d) = \exp(\mathbf{A}d)\mathbf{W}(0) = \mathbf{T}\mathbf{W}(0), \quad (3)$$

where the term $\exp(\mathbf{A}d)$ is the matrix exponential of $\mathbf{A}d$ also known as the transfer matrix \mathbf{T} . Among the different ways of evaluating the matrix exponential [23] is the Padé's approximation. The transfer matrix \mathbf{T} is thus approximated in the long wavelength regime, i.e., when the wavelength λ is much larger than the period d , by

$$\mathbf{T} = \exp(\mathbf{A}d) \sim (\mathbf{I} - \mathbf{A}d/2)^{-1}(\mathbf{I} + \mathbf{A}d/2), \quad (4)$$

where \mathbf{I} is the identity matrix. Assuming the transfer matrix \mathbf{T} between the state vectors at both sides of the unit cell being known, Eq. (4) can be inverted and the expression of the constitutive matrix \mathbf{A} becomes

$$\mathbf{A} \sim d/2(\mathbf{T} + \mathbf{I})^{-1}(\mathbf{T} - \mathbf{I}). \quad (5)$$

The Padé's approximation is of particular interest compared to other approximations such as the Taylor's expansion (see Appendix A), because it allows us to account for the reciprocity of the material [24]. This material property imposes $\det(\mathbf{T}) = 1$, i.e., $t_{11}t_{22} - t_{12}t_{21} = 1$, where t_{ij} are the elements of the matrix \mathbf{T} . Accounting for the reciprocity, Eq. (5) can be rewritten in the form

$$\mathbf{A} \sim \frac{2}{d(2 + t_{11} + t_{22})} \begin{bmatrix} t_{11} - t_{22} & 2t_{12} \\ 2t_{21} & t_{22} - t_{11} \end{bmatrix}, \quad (6)$$

from which we immediately see that the diagonal terms are of opposite signs and we can identify

$$\chi = \frac{-2i(t_{11} - t_{22})}{\omega d(2 + t_{11} + t_{22})}, \quad \rho = \frac{-4it_{12}}{\omega d(2 + t_{11} + t_{22})}, \quad (7)$$

and $\frac{1}{K} = \frac{-4it_{21}}{\omega d(2 + t_{11} + t_{22})},$

by comparison with Eq. (2). Density, bulk modulus and Willis coupling parameter can then be directly calculated via the elements of the transfer matrix that links the state vectors at both sides of the unit cell. Please note that the odd Willis coupling introduced in Ref. [11] is completely canceled from Eq. (6) only because of the reciprocal condition and that only even coupling remains. The effective parameters that are derived following this procedure are indicated by a subscript e in the following.

3. Explicit effective parameters of Willis materials composed of resonant elements

The total transfer matrix \mathbf{T} is evaluated thanks to the knowledge of different elementary transfer matrices that are presented in Appendix B. A circular duct of radius r and length d much smaller than the wavelength is considered. Only plane waves propagate in this duct, i.e., the frequencies are lower than that of the first cut-off of the duct and possible evanescent coupling between the unit cell elements is neglected. The reduced density and bulk modulus (or alternatively the wavenumber and reduced impedance) in the duct are $\bar{\rho}$ and \bar{K} (or alternatively $\bar{k} = k$ and \bar{Z}). Three asymmetric and reciprocal unit cells are considered and are represented in Fig. 1: i) when the duct is loaded by two detuned Helmholtz resonators (HR) located at different positions (Fig. 1(a)) of impedances $\bar{Z}_{HR}^{(j)}$, $j = 1, 2$, ii) when two detuned plates are clamped in the duct (Fig. 1(b)) of impedances $\bar{Z}_p^{(j)}$, $j = 1, 2$, and iii) when the duct is loaded by a HR and a plate is clamped in it at a different position (Fig. 1(c)). Each resonant element possesses its own local dynamics which is assumed different from that of the duct, i.e., co-dynamic regime is assumed [25]. This is an important difference with respect to a laminated two-material unit cell for example, for which it is clear that a second order Taylor expansion of the total matrix elements in Eq. (7) is required to exhibit Willis coupling terms as demonstrated in Appendix C. The order of the resonant element impedances becomes unclear notably around the resonance as explained in Appendix B. Nevertheless, $1/\bar{Z}_{HR}$ (Lorentzian function) and \bar{Z}_p (inverse of a Lorentzian function) are assumed to vary like $\mathcal{O}((kd)^2)$ to ensure reciprocity of the configuration in the considered frequency range, see for example the discussion of Appendix D in the presence of a single HR. Note that this relies more on a frequency analysis rather than on a purely kd analysis.

3.1. Unit cell composed of a duct loaded by two detuned Helmholtz resonators

We first consider a unit cell of length d composed of a straight circular duct loaded by two detuned HR of respective reduced impedances $\bar{Z}_{HR}^{(1)}$ and $\bar{Z}_{HR}^{(2)}$, assumed to be point-like resonators, and located at $l^{(1)}$ and $l^{(1)} + l^{(2)}$ such that $d = l^{(1)} + l^{(2)} + l^{(3)}$, as represented Fig. 1(a). Both inverse impedances $\frac{1}{\bar{Z}_{HR}^{(1)}}$ and $\frac{1}{\bar{Z}_{HR}^{(2)}}$ are assumed to be $\mathcal{O}((kd)^2)$ terms. This configuration is formally that considered in Ref. [3], where the loading quarter-wavelength resonators are replaced by HR. The total transfer matrix reads as

$$\mathbf{W}(d) = \mathbf{T}\mathbf{W}(0) = \mathbf{T}_{l^{(3)}}\mathbf{T}_{HR^{(2)}}\mathbf{T}_{l^{(2)}}\mathbf{T}_{HR^{(1)}}\mathbf{T}_{l^{(1)}}\mathbf{W}(0), \quad (8)$$

where the transfer matrices accounting for the propagation along each length and for the loading HR are given in Eqs. (B.1) and (B.2). Assuming $kd \ll \lambda$, in such a way that $kl^{(1)} = \zeta^{(1)}kd$, $kl^{(2)} = \zeta^{(2)}kd$, and $kl^{(3)} = \zeta^{(3)}kd$, with $\zeta^{(j)} = l^{(j)}/d$, $j = 1, 2, 3$, are

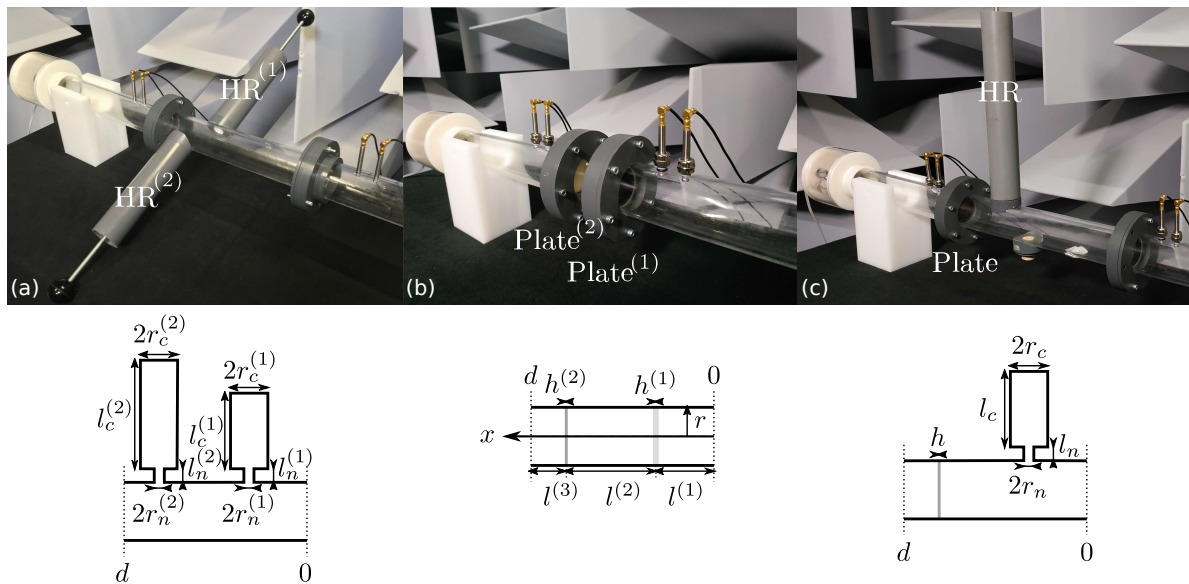


Figure 1. (Color online) Pictures of the three studied Willis unit cells: (a) a straight duct loaded by two detuned HR located at different positions, (b) a straight duct with two detuned plates clamped in it, and (c) a straight duct loaded by a HR and with a plate clamped in it at a different position. A sketch of the configuration is provided below each picture.

also much smaller than the wavelength, and making use of Eq. (7) leads to

$$\begin{aligned}
 \chi_e &= \frac{\bar{\rho}}{2d} \left(\frac{l^{(3)} + l^{(2)} - l^{(1)}}{Z_{HR}^{(1)}} + \frac{l^{(3)} - l^{(1)} - l^{(2)}}{Z_{HR}^{(2)}} \right) + \mathcal{O}((kd)^3), \\
 \rho_e &= \bar{\rho} + \mathcal{O}((kd)^3), \\
 \frac{1}{K_e} &= \frac{1}{\bar{K}} + \frac{1}{d} \left(-\frac{i}{\omega \bar{Z}_{HR}^{(1)}} - \frac{i}{\omega \bar{Z}_{HR}^{(2)}} \right) + \mathcal{O}((kd)^3).
 \end{aligned} \tag{9}$$

To get a grip on these equations, we compare them to those in the presence of a single HR presented in Appendix D. The Willis coupling term appears as the sum of the two Willis coupling terms arising from each HR. Each of them clearly exhibits a momentum introduced by the resonator as testified by the moment arm term $l^{(3)} + l^{(2)} - l^{(1)}$ for the first HR and the moment arm term $l^{(3)} - l^{(1)} - l^{(2)}$ for the second HR. The Willis coupling parameter vanishes when the symmetry is introduced, for example, when the two HR are identical and when $l^{(3)} = l^{(1)}$. It appears in the form of an effective density divided by the impedance of the HR. The density term, second line of Eq.(9), is not the subject of any specific remark and simply reads as the effective density in the duct. The bulk modulus is the sum of the contribution of the effective properties of the duct in the absence of the loading resonators, i.e., $1/\bar{K}$, and of each HR, i.e., $-i/d\omega \bar{Z}_{HR}^{(j)}$, $j = 1, 2$. The presence of the HR causes the effective bulk modulus to become negative for frequencies around their resonances [26, 27]. All in all, the effective parameters appear as the sum of those of each elements, i.e., those of each segments and those of the HR, without any particular coupling. When a subperiodicity can be introduced,

i.e., when the two HR are identical and when $l_2 = d/2$, the effective parameters reduce to those of a unit cell of length $d/2$ consisting in a single, possibly uncentered, HR with Willis parameter exhibiting a moment arm term equal to $l^{(3)} - l^{(1)}$.

3.2. Unit cell composed of a duct with detuned clamped plates

We now consider a unit cell of length d , as depicted in Fig. 1(b), composed of a straight circular duct in which two detuned plates, assumed to be point-like resonators, of respective reduced impedances $\bar{Z}_p^{(1)}$ and $\bar{Z}_p^{(2)}$ are clamped at $l^{(1)}$ and $l^{(1)} + l^{(2)}$ such that $d = l^{(1)} + l^{(2)} + l^{(3)}$. The clamped plates (CP) simply replace the HR when compared to the previous configuration, but this time the impedances are in series instead of being in parallel. This configuration is formally that considered in Ref. [9]. The total transfer matrix reads as

$$\mathbf{W}(d) = \mathbf{TW}(0) = \mathbf{T}_{l^{(3)}} \mathbf{T}_{p^{(2)}} \mathbf{T}_{l^{(2)}} \mathbf{T}_{p^{(1)}} \mathbf{T}_{l^{(1)}} \mathbf{W}(0), \quad (10)$$

where the transfer matrices accounting for the propagation along each length and for the CP are given in Eqs. (B.1) and (B.4). Proceeding similarly as in the previous section, Eq. (7) together with the second order Taylor expansion of the total transfer matrix elements provides

$$\begin{aligned} \chi_e &= \frac{1}{2d\bar{K}} \left(Z_{p^{(1)}} (l^{(1)} - l^{(2)} - l^{(3)}) + \right. \\ &\quad \left. Z_{p^{(2)}} (l^{(1)} + l^{(2)} - l^{(3)}) \right) + \mathcal{O}((kd)^3), \\ \rho_e &= \bar{\rho} + \frac{1}{d} \left(-\frac{iZ_{p^{(1)}}}{\omega} - \frac{iZ_{p^{(2)}}}{\omega} \right) + \mathcal{O}((kd)^3), \\ \frac{1}{K_e} &= \frac{1}{\bar{K}} + \mathcal{O}((kd)^3). \end{aligned} \quad (11)$$

The Willis coupling term appears as the sum of the Willis terms associated with each plate (see Appendix D). The momentum seems opposite to that imposed by the HR with an arm term $l^{(1)} - l^{(2)} - l^{(3)}$ for the first CP and an arm term $l^{(1)} + l^{(2)} - l^{(3)}$ for the second CP. It appears in the form of an effective compressibility multiplied by the impedance of the plate. Again, this term vanishes when the symmetry is introduced as for example, when the two CP are identical and $l^{(3)} = l^{(1)}$. The density is the sum of the contribution of the effective density of the duct in the absence of the CP, i.e., $\bar{\rho}$, and of each CP, i.e., $-iZ_{p^{(j)}}/d\omega$, $j = 1, 2$. The presence of the clamped plates causes the density to be negative for frequencies lower than their resonances [28]. Finally, the effective bulk modulus is that in the absence of the clamped plate and is thus not the subject of any specific remark. The effective parameters again appear as the sum of those of each elements, i.e., those of each segments and those of the CP, without any particular coupling. When a plane of symmetry can be introduced, i.e., when the two CP are identical and when $l_2 = d/2$, the effective parameters reduce to those of a unit cell of length $d/2$ consisting in a single, possibly uncentered, CP with Willis parameter exhibiting a moment arm term equal to $l^{(1)} - l^{(3)}$.

3.3. Unit cell composed of a duct with a clamped plate and loaded by a detuned Helmholtz resonator

We finally consider a unit cell of length d composed of a straight circular duct in which a plate, assumed to be a point-like resonator, of reduced impedance \bar{Z}_p is clamped at $l^{(1)}$. The duct is in addition loaded by a HR, also assumed to be a point-like resonator, of reduced impedance \bar{Z}_{HR} and located at $l^{(1)} + l^{(2)}$ such that $d = l^{(1)} + l^{(2)} + l^{(3)}$. A picture of the configuration is shown in Fig. 1(c). In other words, the first HR is replaced by a CP compared to the configuration studied in Section 3.1 or the second CP is replaced by a HR compared to the configuration studied in Section 3.2. Beyond the expected double negative effective property [29], this asymmetric configuration combines impedances in series and in parallel and is similar to that studied in Ref. [11]. The total transfer matrix reads as

$$\mathbf{W}(d) = \mathbf{TW}(0) = \mathbf{T}_{l^{(3)}} \mathbf{T}_{HR} \mathbf{T}_{l^{(2)}} \mathbf{T}_p \mathbf{T}_{l^{(1)}} \mathbf{W}(0), \quad (12)$$

where the transfer matrices accounting for the propagation along each length, for the CP, and for the HR are given in Eqs. (B.1), (B.4), and (B.2) respectively. Again, Eq. (7) together with the second order Taylor expansion of the total transfer matrix elements provides

$$\begin{aligned} \chi_e &= \frac{1}{2d} \left(\frac{\bar{\rho}}{Z_{HR}} (l^{(3)} - l^{(1)} - l^{(2)}) + \frac{Z_p}{\bar{K}} (l^{(1)} - l^{(2)} - l^{(3)}) + \frac{iZ_p}{\omega Z_{HR}} \right) + \mathcal{O}((kd)^3), \\ \rho_e &= \bar{\rho} - \frac{iZ_p}{d\omega} + \mathcal{O}((kd)^3), \\ \frac{1}{K_e} &= \frac{1}{\bar{K}} - \frac{i}{d\omega Z_{HR}} + \mathcal{O}((kd)^3). \end{aligned} \quad (13)$$

Contrary to the configurations studied in both previous sections, the Willis coupling term is not only the sum of the Willis terms associated with the presence of the CP and of the HR (see Appendix D), but also exhibits a coupling between the CP and the HR thanks to the term $iZ_p/2d\omega Z_{HR}$. Note that the moment arms are introduced by the first two terms, that related to the presence of the CP and that related to the presence HR, while the coupling term does not present moment arm term. In addition, the Willis coupling parameter never seems to vanish, because the configuration is structurally asymmetric. The density is the sum of the contribution of the effective density of the duct in the absence of the CP and of the HR, and of the CP, i.e., $-iZ_p/d\omega$. In a similar way, the bulk modulus is the sum of the contribution of the effective bulk modulus of the duct in the absence of the CP and of the HR, and of the HR, i.e., $-i/d\omega Z_{HR}$. Note that obviously no symmetry plane can be introduced for this configuration.

4. Experimental validation of the effective parameters and discussion

All experiments are conducted in a duct of radius $r = 2.5$ cm, see Figs. 1(a-c). The experimental set-up consists of a 4 microphone measurement system with a pair of

microphones upstream and a second pair of microphones downstream of the sample. The microphones that compose each pair are separated by a distance of 2.5 cm. A stepped signal from 100 Hz to 1000 Hz with a step of 1 Hz is delivered by a loudspeaker at one end of the duct and an anechoic termination is mounted at the opposite end. Temperature, humidity and atmospheric pressure are recorded for each experiment. The transfer function between the loudspeaker and each microphone is recorded by a NI USB-4431 acquisition card driven by the INTAC software. Each sample is measured in both direct and reverse orientations in order to form an overdetermined system based on the scattering matrix [30, 3] as explained in Appendix E to solve for T , R^+ , and R^- , i.e., the transmission, the direct orientation reflection, and the reverse orientation reflection coefficients. These coefficients are also calculated by the Transfer Matrix Method (TMM) using the total transfer matrix relying on the elementary matrices and the Pade's approximation of transfer matrix relying on the evaluated effective parameters $(\mathbf{I} - \mathbf{A}_e d/2)^{-1} (\mathbf{I} + \mathbf{A}_e d/2)$, Eq. (4),

$$\begin{aligned} R^+ &= \frac{t_{11} - t_{12}/\bar{Z} + \bar{Z}t_{21} - t_{22}}{t_{11} - t_{12}/\bar{Z} - \bar{Z}t_{21} + t_{22}}, & R^- &= \frac{-t_{11} - t_{12}/\bar{Z} + \bar{Z}t_{21} + t_{22}}{t_{11} - t_{12}/\bar{Z} - \bar{Z}t_{21} + t_{22}}, \\ T &= \frac{2}{t_{11} - t_{12}/\bar{Z} - \bar{Z}t_{21} + t_{22}}, \end{aligned} \quad (14)$$

where \bar{Z} is the reduced impedance of the surrounding medium. From the measured direct and inverse orientation reflection and transmission coefficients, the effective parameters are reconstructed following the procedure described in Appendix F. The effective properties can also be directly evaluated from the total transfer matrix as explained in Appendix G, which appears as a numerical version of the procedure described in Ref. [13].

Figures 2(a-e-i) depict respectively the absolute values of the two reflection and transmission coefficients, calculated by the TMM with the total transfer matrix and by the Pade's approximation using the effective properties derived in Section 3 for the three configurations considered in the present article. A single unit cell is measured for each configuration. This measurement is entirely sufficient, because one-dimensional structures are assumed. The first configuration (see Fig. 1(a)) consists in two detuned HR, the dimensions of the cavities and necks of which are $l_c^{(1)} = 8$ cm, $l_c^{(2)} = 4.2$ cm and $r_c^{(1)} = r_c^{(2)} = 2.15$ cm, and $l_n^{(1)} = l_n^{(2)} = 2$ cm and $r_n^{(2)} = r_n^{(1)} = 3$ mm, separated by a distance $l^{(2)} = 5$ cm. The resonant frequencies of both HR are thus $f_{HR}^{(1)} \approx 165$ Hz and $f_{HR}^{(2)} \approx 230$ Hz. The two remaining dimensions $l^{(1)}$ and $l^{(3)}$ are chosen identical, i.e., $l^{(1)} = l^{(3)} = 1$ cm, such that $d = 7$ cm. The second configuration (see Fig. 1(b)) consists in two CP separated by a distance $l^{(2)} = 5$ cm + $(h_p^{(1)} + h_p^{(2)})/2$. The first CP is a plastic shim plate of thickness $h_p^{(1)} = 254$ μ m and material properties $\rho_p^{(1)} = 1400$ kg.m⁻³, $\nu_p^{(1)} = 0.41$, and $E_p^{(1)} = 4.6(1 - 0.03i)$ GPa already used in Ref. [31]. The second CP is a poroelastic plate of thickness $h_p^{(2)} = 3.1$ mm and material properties $\rho_p^{(2)} = 40 + 380i/\sqrt{\omega}$ kg.m⁻¹, $\nu_p^{(2)} = 0.1$, and $E_p^{(2)} = 470 - 0.007i\omega$ kPa already used in Ref. [32]. The resonant frequencies of both CP are thus $f_p^{(1)} \approx 380$ Hz and

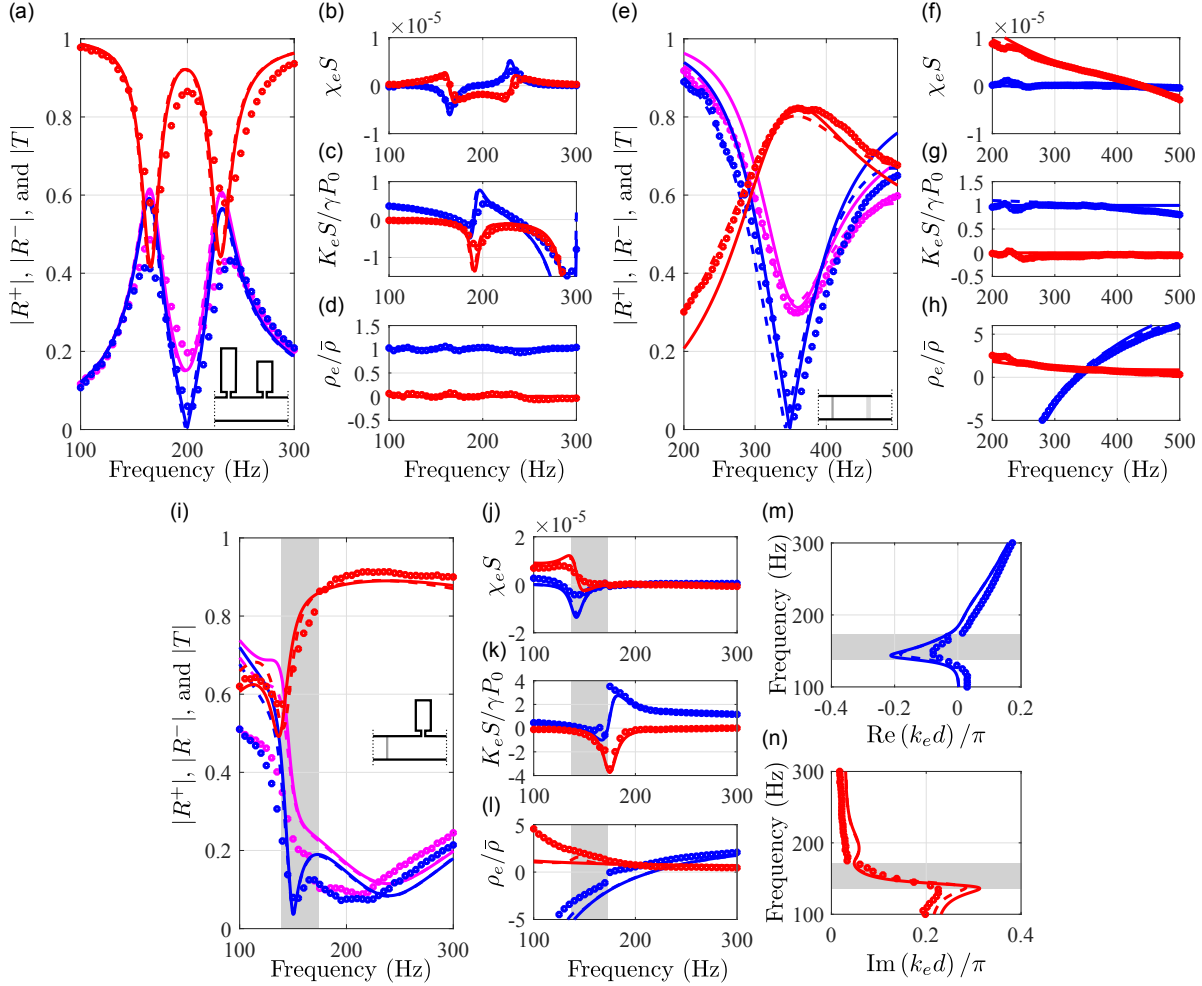


Figure 2. (Color online) (a-e-i) $|R^+|$ (blue curve), $|R^-|$ (magenta curve), and $|T|$ (red curve) as calculated with TMM with the total transfer matrix (dashed line), with the effective parameters (solid line), and as measured experimentally (markers), for a unit cell that is composed of a straight duct loaded by two detuned HR - with two detuned plates clamped in it - with a plate clamped in it and loaded by a detuned HR. Subfigures (b-f-j), (c-g-k) and (d-h-l) depict respectively the real (blue curve) and imaginary (red curve) of the corresponding Willis coupling parameter, normalized density, and normalized bulk modulus. Subfigures (m-n) depict both the real and imaginary parts of the normalized dispersion relation for a unit cell composed of a straight duct with a plate clamped in it and loaded by a detuned HR. The grey regions highlight the frequency band where the real parts of both the effective density and bulk modulus are negative.

$f_p^{(2)} \approx 255$ Hz and the two remaining dimensions $l^{(1)}$ and $l^{(3)}$ are chosen almost identical, i.e., $l^{(1)} = 5$ mm + $h_p^{(1)}/2$ and $l^{(3)} = 5$ mm + $h_p^{(2)}/2$, such that $d = 6$ cm + $h_p^{(1)} + h_p^{(2)}$. The last configuration (see Fig. 1(c)) is composed of the proelastic plate and a loading HR, the cavity and neck dimensions of which are $l_c = 5$ cm and $r_c = 2.15$ cm, and $l_n = 2$ cm and $r_n = 2$ mm, separated by a distance $l^{(2)} = 5$ cm + $h_p/2$. The resonance frequency of the CP is still $f_p = 255$ Hz and that of the HR is $f_{HR} = 140$ Hz and the two remaining dimensions $l^{(1)}$ and $l^{(3)}$ are again chosen almost identical, i.e., $l^{(1)} = 1$ cm + $h_p/2$ and

$l^{(3)} = 1$ cm, such that $d = 7$ cm + h_p . The lengths of the unit cells are thus much smaller than the wavelengths over the frequency range considered in each configuration. The necks were manufactured by Fused Deposition Modeling to fit in an initial radius of 1 cm. The necks also present some rugosity inherent to this rapid manufacturing technique, which can influence the viscothermal losses in these resonator narrow elements [33]. The configurations were designed to present a reflection coefficient that vanishes at a specific frequency while the reflection coefficient of the reverse sample is different from zero at this frequency. The calculated coefficients are found in very good agreement with the experiments, which therefore valid the derived effective properties and prove the asymmetry of the acoustic response of each configuration. Some discrepancies are visible, notably for the third configuration at very low frequencies. These discrepancies are attributed to measurement complexity at low frequencies and to possible evanescent coupling between the resonant elements that is not accounted for in our modeling. At high frequency, the calculated transmission coefficient based on the effective parameters starts to deviate from its value for the second configuration because the scale separation is not ensured anymore and the Pade's approximation is not valid anymore, see Fig. 2(e). In addition, slight shifts between the coefficients calculated with the total transfer matrix and with the effective parameters can also be notice at low frequencies and around the resonances, see Fig. 2(e) and (j). These discrepancies are attributed to the assumption we made on the dependency of the resonant element impedances, that are supposed to vary like kd . Around the resonances, this assumption is not fully valid and the effective properties would require additional terms to be Taylor expanded to the second order.

The normalized effective properties, i.e., $\chi_e S$, $\bar{\rho}_e/\bar{\rho}$, and $K_e S/\gamma P_0$, are respectively depicted in Figs. 2(b-f-j), (c-g-k), and (d-h-l) for each configuration. The numerical and experimental effective properties match those evaluated in Section 3. Generally speaking, the real parts of the effective densities (CP) and bulk moduli (HR) are negative in stop bands and follow regular trends [26, 27, 28, 29]. Some discrepancies are visible for the third configuration again due to the fact that the phenomenon are encountered at very low frequencies, but also to the assumption made on the order of the resonant element impedances. The amplitude of the Willis parameter is usually much smaller than the other ones, partially due to the fact that this parameter is only normalized by the cross-sectional area of the main duct S , in the absence of a normalization value for this parameter. Note that $\chi_e S$ vanishes away from the resonances in case of detuned HR, while it tends to infinity at low frequency when a plate is involved, see Figs. 2(f,j). A similar remark is made concerning the effective density $\bar{\rho}_e/\bar{\rho}$. This is due to the presence of the term \bar{Z}_p in both χ_e and ρ_e , Eqs. (11) and (13), which varies like $1/\omega$ at low frequencies. This also blurs the required order of Taylor expansion to derive these effective parameters even away from the resonances in case of unit cells involving plates as it can be seen in Figs. 2(e) and 2(i). This divergence is nevertheless physical, because a plate should be a rigid wall at low frequency. Note that to reach the request accuracy too near to resonance, non-local effective medium are probably requested, which are outside the scope of the current paper. The dispersion relation is also plotted for the

configuration comprising a straight duct with a CP and loaded by a detuned HR in Figs. 2(m-n). The grey areas highlight the frequency range where the real parts of both the effective density and bulk modulus are negative. The viscothermal losses and Willis coupling induce a slight shift in the negative index part. The dispersion relation for the other two configurations (not shown here) are found in good agreement.

5. Conclusion

We derive closed forms of the effective properties of Willis materials thanks to a Pade's approximation of the total transfer matrix linking the state vectors at both sides of an asymmetric and reciprocal one-dimensional unit cell. We primarily show that the reciprocal condition leads to the unique existence of the even Willis coupling. Similarly to the case of laminated structures, which are usually in nonresonant acoustic structures, second order Taylor expansion of the transfer matrix elements is sufficient to exhibit Willis coupling parameters. Nevertheless, this result relies on a strong assumption on the resonant element behavior and its veracity is questioned around the resonance. Higher order Taylor expansion of the full transfer matrix terms involving the resonant elements may therefore be more suitable. The dipolar feature of the Willis coupling is clearly evidenced, because the coupling parameter presents moment arm terms. This also links Willis material to higher order strain gradient theories [34]. We also evidenced different types of coupling terms due to the asymmetry, either absent when the unit cell consists in detuned identical type resonators or due to a physical asymmetry when the unit cell involves different types of resonators. Beyond the derivation of these closed-forms, we also show that various asymmetric structures can be modeled as Willis materials. Each effective parameter (effective density, effective bulk modulus, and effective Willis coupling parameter) is validated against experimental and numerical results, showing the robustness of the derivation method. This work paves the way for the engineering use of Willis materials, from perfect absorption devices in transmission problems, to double negative structures, but also to metaporous materials and liquid foams [35, 36, 37].

Acknowledgments

J.-P.G., M.M., V.R.-G., and V.T. would like to thank the support of the ANR-RGC METARoom project (ANR-18-CE08-0021). J.L. would like to thank the support of the Research Grants Council in Hong Kong (Grant No. 16302218). D.T. acknowledges financial support through the "Ramón y Cajal" fellowship under grant number RYC-2016-21188.

Appendix A. Padé's approximation versus Taylor's expansion

In the long-wavelength regime, the first order Taylor's expansion of the transfer matrix reads as

$$\mathbf{T} = \exp(\mathbf{A}d) \sim \mathbf{I} + \mathbf{A}d, \quad (\text{A.1})$$

which can be inverted to provide

$$\begin{aligned} \mathbf{A} &\sim \frac{1}{d} (\mathbf{T} - \mathbf{I}) \\ &\sim \frac{1}{d} \begin{bmatrix} t_{11} - 1 & t_{12} \\ t_{21} & t_{22} - 1 \end{bmatrix}. \end{aligned} \quad (\text{A.2})$$

This expression does not ensure the reciprocity of the material and the diagonal terms are not opposite each other. Taylor's expansion, at least of first order, is not a sufficiently robust tool to derive effective parameters, when compared to Padé's approximation.

Appendix B. Elementary transfer matrices

This section details the different elementary transfer matrices that are used to evaluate the total transfer matrix \mathbf{T} .

Appendix B.1. Propagation in a duct of length l

The elementary matrix \mathbf{T}_l that connects the state vectors at two locations separated from a length l in a straight duct of section S reads as

$$\mathbf{W}(l) = \mathbf{T}_l \mathbf{W}(0) = \exp(\mathbf{A}l) \mathbf{W}(0) = \begin{bmatrix} \cos(kl) & i\bar{Z} \sin(kl) \\ \frac{i \sin(kl)}{\bar{Z}} & \cos(kl) \end{bmatrix} \mathbf{W}(0), \quad (\text{B.1})$$

where $k = \omega/c = \omega/\sqrt{\bar{K}/\bar{\rho}}$ is the wavenumber, $\bar{K} = K/S$, $\bar{\rho} = \rho/S$ and $\bar{Z} = \sqrt{\bar{K}\bar{\rho}}$ are respectively the reduced bulk modulus, density and impedance.

Appendix B.2. Impedance in parallel

A flow split at a position s associated with the continuity of pressure is modeled by an impedance Z_{HR} in parallel leading to an elementary matrix \mathbf{T}_{HR}

$$\mathbf{W}(s) = \mathbf{T}_{HR} \mathbf{W}(s) = \begin{bmatrix} 1 & 0 \\ 1/\bar{Z}_{HR} & 1 \end{bmatrix} \mathbf{W}(s). \quad (\text{B.2})$$

In particular, the impedance of a side branch HR to a duct of radius r , assumed to be a point-like resonator, is [38]

$$\bar{Z}_{HR} = \frac{-i\bar{Z}_n \left(1 - k_n \frac{\bar{Z}_n}{\bar{Z}_c} \delta \tan(k_n l_c) - \frac{\bar{Z}_n}{\bar{Z}_c} \tan(k_n l_n) \tan(k_n l_c) \right)}{\tan(k_n l_n) - k_n \frac{\bar{Z}_n}{\bar{Z}_c} \delta \tan(k_n l_n) \tan(k_n l_c) + \frac{\bar{Z}_n}{\bar{Z}_c} \tan(k_n l_c)}, \quad (\text{B.3})$$

where k_n and \bar{Z}_n are respectively the wavenumber and reduced impedance of the neck, k_c and \bar{Z}_c are respectively the wavenumber and reduced impedance of the cavity, and $\delta = 0.82(1 - 1.35r_n/r_c + 0.31(r_n/r_c)^3)r_n + 0.82(1 - 0.235r_n/r - 1.32(r_n/r)^2 + 1.54(r_n/r)^3 - 0.86(r_n/r)^4)r_n$ is the correction length, with r_n and r_c the radius of the neck and of the cavity respectively.

In the absence of losses and correction length, the latter impedance reduces to $\bar{Z}_{HR} = -iZ(1 - k^2 l_n S_c l_c / S_n) / k(S_n l_n + S_c l_c)$ at low frequencies, from which it follows that $1/\bar{Z}_{HR}$ varies like ω when $\omega \rightarrow 0$, but like a Lorentzian around the resonance frequency.

Appendix B.3. Impedance in series

A pressure drop at a position s associated with the continuity of the normal velocity (or flow) is modeled by an impedance Z_p in series leading to an elementary matrix \mathbf{T}_p

$$\mathbf{W}(s) = \mathbf{T}_p \mathbf{W}(s) = \begin{bmatrix} 1 & \bar{Z}_p \\ 0 & 1 \end{bmatrix} \mathbf{W}(s). \quad (\text{B.4})$$

In particular, the impedance of a h_p -thick plate clamped in a circular duct of radius r and section S , assumed to be a point-like resonator, is [39]

$$\bar{Z}_p = \frac{-i\omega\rho_p h_p I_1(k_p r) J_0(k_p r) - I_0(k_p r) J_1(k_p r)}{S I_1(k_p r) J_2(k_p r) + I_2(k_p r) J_1(k_p r)}, \quad (\text{B.5})$$

where I_n and J_n are respectively the modified and regular Bessel functions of first kind and order n , and ρ_p and k_p are respectively the density and wavenumber of the plate. The wavenumber is $k_p^4 = \omega^2 \rho_p h_p / D_p$, where $D_p = E_p h_p^3 / 12 (1 - \nu_p^2)$ is the bending stiffness, with E_p and ν_p the Young's modulus and Poisson's ratio of the plate material respectively. Note that poroelastic and viscoelastic plates can be modeled with a complex and frequency dependent Young's modulus and/or density.

The plate impedance reduces to $\bar{Z}_p = -i\omega 192\rho_p h_p (1/(k_p r)^4 - 5/384) / S$ at low frequencies, from which it follows that \bar{Z}_p varies like $1/\omega$ when $\omega \rightarrow 0$ because a plate tends to a rigid wall ($\bar{Z}_p \rightarrow \infty$) at low frequency, like the inverse of a Lorentzian around the resonance frequency, and like ω otherwise.

Appendix B.4. Viscothermal losses

Circular ducts are considered all along this article. The boundaries give rise to viscothermal losses from viscous and thermal skin depths. Assuming that only plane waves propagate in a circular duct of radius r , the effective complex and frequency

dependent density and bulk modulus read as [40]

$$\begin{aligned} \rho &= \rho_0 \left(1 - \frac{2}{r\sqrt{i\omega\rho_0/\eta}} \frac{J_1\left(r\sqrt{i\omega\rho_0/\eta}\right)}{J_0\left(r\sqrt{i\omega\rho_0/\eta}\right)} \right)^{-1}, \\ K &= \gamma P_0 \left(1 + \frac{2(\gamma-1)}{r\sqrt{iPr\omega\rho_0/\eta}} \frac{J_1\left(r\sqrt{iPr\omega\rho_0/\eta}\right)}{J_0\left(r\sqrt{iPr\omega\rho_0/\eta}\right)} \right)^{-1}, \end{aligned} \quad (\text{B.6})$$

where ρ_0 , γ , η , and Pr are respectively the density, specific heat ratio, dynamic density and Prandtl number of the saturating fluid, and P_0 the atmospheric pressure. The reduced density and bulk modulus can then be straightforwardly evaluated by $\bar{\rho} = \rho/S$ and $\bar{K} = K/S$, with $S = \pi r^2$.

Appendix C. Derivation of the Willis parameters in the case of a laminated two-material unit cell

We assume a unit cell of length d composed of a material $M^{(1)}$ of density $\rho^{(1)}$ and bulk modulus $K^{(1)}$ and of length $l^{(1)}$ and a material $M^{(2)}$ of density $\rho^{(2)}$ and bulk modulus $K^{(2)}$ and of length $l^{(2)} = d - l^{(1)}$. The state vectors at both sides of the unit cell are thus related by the total transfer matrix composed of the multiplication of the transfer matrix modeling the propagation in the material $M^{(1)}$ over the length $l^{(1)}$ and that in the material $M^{(2)}$ over the length $l^{(2)}$

$$\mathbf{W}(d) = \mathbf{T}\mathbf{W}(0) = \mathbf{T}_{l^{(2)}}\mathbf{T}_{l^{(1)}}\mathbf{W}(0), \quad (\text{C.1})$$

where the expression of $\mathbf{T}_{l^{(2)}}$ and of $\mathbf{T}_{l^{(1)}}$ are given Eq. (B.1). Assuming $kd \ll \lambda$, in such a way that $k^{(1)}l^{(1)} = \zeta^{(1)}kd$ and $k^{(2)}l^{(2)} = \zeta^{(2)}kd$, with $\zeta^{(j)} = l^{(j)}/d$, $j = 1, 2$, are also much smaller than the wavelength and making use of Eq. (7) leads to

$$\begin{aligned} \chi_e &= 0 + \mathcal{O}((kd)^2), \quad \rho_e = \frac{1}{d} (l^{(2)}\rho^{(2)} + l^{(1)}\rho^{(1)}) + \mathcal{O}((kd)^2), \\ \text{and } \frac{1}{K_e} &= \frac{1}{d} \left(\frac{l^{(2)}}{K^{(2)}} + \frac{l^{(1)}}{K^{(1)}} \right) + \mathcal{O}((kd)^2), \end{aligned} \quad (\text{C.2})$$

if we only Taylor expand the elements of the transfer matrix to the first order. In the opposite, it leads to

$$\begin{aligned} \chi_e &= \frac{i\omega l^{(1)}l^{(2)}}{2d} \left(\frac{\rho^{(2)}}{K^{(1)}} - \frac{\rho^{(1)}}{K^{(2)}} \right) + \mathcal{O}((kd)^3), \\ \rho_e &= \frac{1}{d} (l^{(2)}\rho^{(2)} + l^{(1)}\rho^{(1)}) + \mathcal{O}((kd)^3), \\ \frac{1}{K_e} &= \frac{1}{d} \left(\frac{l^{(2)}}{K^{(2)}} + \frac{l^{(1)}}{K^{(1)}} \right) + \mathcal{O}((kd)^3), \end{aligned} \quad (\text{C.3})$$

if we Taylor expand the elements of the transfer matrix to the second order. Of particular interest is the fact that the eigenvalues of \mathbf{A}_e , i.e., the wavevectors, are identical for both orders of expansion (assuming respectively first and second order expansion) and equal to $k_e = \pm \frac{i\omega}{\sqrt{K_e/\rho_e}}$, while the eigenvectors exhibit $Z_e^\pm = K_e(k_e \pm \chi_e)$ at the second order

against $Z_e^\pm = K_e k_e$ at the first order. In the lossless case, the Willis coupling parameter is purely imaginary.

Appendix D. Derivation of the Willis parameters in case of a unit cell presenting a single resonator

This section is motivated by nonlocal aspects of the Willis coupling and the fact that structures are often bounded in practice. Moreover, it helps in a better understanding of coupling terms that arise in case of more complex asymmetric unit cells.

Appendix D.1. Derivation of the Willis parameters in case of a unit cell presenting a single Helmholtz resonator

We consider a unit cell composed of a straight duct of length d and radius r loaded by a HR of reduced impedance \bar{Z}_{HR} and located at $l^{(1)}$ such that $d = l^{(1)} + l^{(2)}$. The total transfer matrix reads as

$$\mathbf{W}(d) = \mathbf{T}\mathbf{W}(0) = \mathbf{T}_{l^{(2)}}\mathbf{T}_{HR}\mathbf{T}_{l^{(1)}}\mathbf{W}(0), \quad (\text{D.1})$$

where the transfer matrix accounting for the propagation along each length and the HR are provided in Eqs. (B.1) and (B.2). Assuming $kd \ll \lambda$, in such a way that $kl^{(1)} = \zeta^{(1)}kd$ and $kl^{(2)} = \zeta^{(2)}kd$, with $\zeta^{(j)} = l^{(j)}/d$, $j = 1, 2$, are also much smaller than the wavelength, but also that $1/\bar{Z}_{HR}$ is a $\mathcal{O}((kd)^2)$ term (because it varies like ω at low frequencies), and making use of Eq. (7) leads to

$$\begin{aligned} \chi_e &= \frac{1}{2d} \left(\frac{\bar{\rho}^{(2)}l^{(2)} - \bar{\rho}^{(1)}l^{(1)}}{Z_{HR}} + i\omega l^{(2)}l^{(1)} \left(\frac{\bar{\rho}^{(2)}}{\bar{K}^{(1)}} - \frac{\bar{\rho}^{(1)}}{\bar{K}^{(2)}} \right) \right) + \mathcal{O}((kd)^3) \\ &= \frac{\bar{\rho}}{2d} \frac{l^{(2)} - l^{(1)}}{Z_{HR}} + \mathcal{O}((kd)^3), \\ \rho_e &= \frac{1}{d} (\bar{\rho}^{(1)}l^{(1)} + \bar{\rho}^{(2)}l^{(2)}) + \mathcal{O}((kd)^3), \\ &= \bar{\rho} + \mathcal{O}((kd)^3), \\ \frac{1}{K_e} &= \frac{1}{d} \left(\frac{l^{(1)}}{\bar{K}^{(1)}} + \frac{l^{(2)}}{\bar{K}^{(2)}} - \frac{i}{\omega \bar{Z}_{HR}} \right) + \mathcal{O}((kd)^3). \\ &= \frac{1}{\bar{K}} - \frac{i}{\omega \bar{Z}_{HR}d} + \mathcal{O}((kd)^3). \end{aligned} \quad (\text{D.2})$$

At first glance, the effective parameters appear as the sum of those of a laminated two-material unit cell, Eqs. (C.3) and additional terms related to the presence of the HR. The main tube is identical along the segments 1 and 2, thus $\bar{K}^{(1)} = \bar{K}^{(2)}$ and $\bar{\rho}^{(1)} = \bar{\rho}^{(2)}$ making the Willis parameter associated with the two materials to collapse. The effective bulk modulus and density then read as those proposed in [26, 27]. The presence of the HR affects the bulk modulus, which can become negative around the HR resonance. The Willis parameter only accounts the possible phase shift, when a material is bounded by bounds that do not coincide with the natural unit cell bounds, i.e., when the HR cannot be centered in the unit cell. Please note that the Willis parameter simply vanishes when $l^{(1)} = l^{(2)} = d/2$. Nevertheless, the term $l^{(2)} - l^{(1)}$ translates a momentum within the

unit cell. While ρ_e and $1/K_e$ are also $\mathcal{O}((kd)^2)$ terms, χ_e is a $\mathcal{O}((kd)^3)$ term, when $1/\bar{Z}_{HR}$ is assumed to be a $\mathcal{O}((kd)^2)$ term.

To prove that $1/\bar{Z}_{HR}$ should be a $\mathcal{O}((kd)^2)$ term (at least in the low frequency), we adopt a *reductio ad absurdum*. Let us assume a centered HR (i.e., the Willis parameter vanishes) and that $1/\bar{Z}_{HR}$ is a $\mathcal{O}(kd)$ term for example. The Eqs. (D.2) are thus derived from a first order Taylor expansion of the elements of the total transfer matrix. Under these assumptions, $\det(\mathbf{T}) \approx 1 - i\omega\bar{\rho}d/\bar{Z}_{HR} + \mathcal{O}((kd)^2) \neq 1$ does not satisfy the reciprocity condition. Thus, $1/\bar{Z}_{HR}$ is assumed to be a $\mathcal{O}((kd)^2)$ term. Note that this relies more on a frequency analysis rather than on a kd analysis. We will therefore use the power of ω instead of the power of kd to express the order of Taylor expansion in the following.

Appendix D.2. Derivation of the Willis parameters in the case of a unit cell presenting a single clamped plate

We consider a unit cell composed of a straight duct of length d and radius r in which a plate of reduced impedance \bar{Z}_p is clamped at $l^{(1)}$ such that $d = l^{(1)} + l^{(2)}$. The total transfer matrix reads as

$$\mathbf{W}(d) = \mathbf{T}\mathbf{W}(0) = \mathbf{T}_{l^{(2)}}\mathbf{T}_p\mathbf{T}_{l^{(1)}}\mathbf{W}(0), \quad (\text{D.3})$$

where the transfer matrix accounting for the propagation along each length and the CP are provided in Eqs. (B.1) and (B.4). Assuming $kd \ll \lambda$, in such a way that $kl^{(1)} = \zeta^{(1)}kd$ and $kl^{(2)} = \zeta^{(2)}kd$, again with $\zeta^{(j)} = l^{(j)}/d$, $j = 1, 2$, are also much smaller than the wavelength, but also that \bar{Z}_p is a $\mathcal{O}((kd)^2)$ term (because it varies like ω at low frequencies), and making use of Eq. (7) leads to

$$\begin{aligned} \chi_e &= \frac{\bar{Z}_p}{2d} \frac{l^{(1)} - l^{(2)}}{\bar{K}} + \mathcal{O}((kd)^3), \\ \rho_e &= \bar{\rho} - \frac{i\bar{Z}_p}{\omega d} + \mathcal{O}((kd)^3), \\ \frac{1}{K_e} &= \frac{1}{\bar{K}} + \mathcal{O}((kd)^3). \end{aligned} \quad (\text{D.4})$$

The effective bulk modulus and density read as those proposed in [28]. The presence of the CP affects the density, which can become negative around the resonance. The Willis parameter only accounts the possible phase shift, when a material is bounded by bounds that do not coincide with the natural unit cell bounds, i.e., when the CP cannot be centered in the unit cell. Please note that the Willis parameter simply vanishes when $l^{(1)} = l^{(2)} = d/2$. Nevertheless, the term $l^{(1)} - l^{(2)}$ translates a momentum within the unit cell. Note that the fact that the main tube is identical along the 1 and 2 segments has already been accounted for and that an analysis similar to that performed in Appendix D.1 can be carried out to prove that \bar{Z}_p should be assumed to be a $\mathcal{O}((kd)^2)$ term. Nevertheless, this assumption is even more tedious than that made in the case of the Helmholtz resonator, because \bar{Z}_p physically diverges at very low frequency.

Appendix E. Measurement of the direct and reverse orientation reflection and transmission coefficients

Let us label the upstream and downstream 1/4 in Grass microphones 1, 2, 3, and 4 from the loudspeaker to the anechoic end. The pressure p_j is thus recorded at location x_j , the first interface of the structure is located at x_s and the structure is of length d . A method based on the scattering matrix is preferred, because anechoic termination is never fully anechoic and thus back propagating waves are always present due to reflection at the end of duct [30]. The ingoing i and outgoing o waves at the interfaces of the samples (vanishing phase is imposed at these interfaces) can thus be reconstructed to form the first set of equations

$$\begin{cases} p_u^o = R^+ p_u^i + T p_d^i, \\ p_d^o = T p_u^i + R^- p_d^i. \end{cases} \quad (\text{E.1})$$

Turning the sample over and repeating the procedure (second set of measurements are mark with '), gives another set of equations

$$\begin{cases} p_u^{o'} = R^- p_u^{i'} + T p_d^{i'}, \\ p_d^{o'} = T p_u^{i'} + R^+ p_d^{i'}. \end{cases} \quad (\text{E.2})$$

These two sets of equations form an overdetermined system to solve for R^+ , R^- , and T .

Appendix F. Recovery procedure of the effective parameters from the measured reflection and transmission coefficients

The two state vectors at both sides of the sample are related by

$$\begin{aligned} \mathbf{W}(d) &= \exp(\mathbf{A}d) \mathbf{W}(0) \\ &= \mathbf{V} \text{diag} \left(e^{\Sigma^\pm d} \right) \mathbf{V}^{-1} \mathbf{W}(0), \end{aligned} \quad (\text{F.1})$$

where diag is the diagonal matrix, Σ^\pm are the eigenvalues of \mathbf{A} and \mathbf{V} the corresponding eigenvector matrix. For a Willis material, the constitutive matrix of which is given in Eq. (2), $\Sigma^\pm = \pm i\omega \sqrt{\chi^2 + \rho/K} = \pm i\omega\sigma$,

$$\begin{aligned} \mathbf{V} &= \frac{1}{\sqrt{2}} \begin{bmatrix} K(\chi + \sigma) & K(\chi - \sigma) \\ 1 & 1 \end{bmatrix}, \text{ and} \\ \mathbf{V}^{-1} &= \frac{1}{\sqrt{2}} \begin{bmatrix} 1/K\sigma & (\sigma - \chi)/\sigma \\ -1/K\sigma & (\sigma + \chi)/\sigma \end{bmatrix}. \end{aligned} \quad (\text{F.2})$$

Introducing R^+ , R^- , and T in the state vectors Eq. (F.1) leads to 2 systems of equations

$$\begin{aligned} \begin{bmatrix} 1 + R^+ \\ \frac{-1 + R^+}{Z} \end{bmatrix} &= \exp(\mathbf{A}d) \begin{bmatrix} T \\ \frac{-T}{Z} \end{bmatrix}, \text{ and} \\ \begin{bmatrix} T \\ \frac{T}{Z} \end{bmatrix} &= \exp(\mathbf{A}d) \begin{bmatrix} 1 + R^- \\ \frac{1 - R^-}{Z} \end{bmatrix}. \end{aligned} \quad (\text{F.3})$$

Introducing $r^\pm = (Z + Z^\pm)/(Z - Z^\pm)$, where $Z^\pm = K(\sigma \pm \chi)$, the reflection coefficients at the interface between a semi-infinite background medium (of impedance Z) and the Willis material in the direct and reverse orientations, these equations can be inverted to yield

$$\begin{aligned} r^+ &= \frac{-(R^- R^+ + 1 - T^2) \pm \sqrt{(R^- R^+ + 1 - T^2)^2 - 4R^- R^+}}{2R^+}, \\ r^- &= \frac{-(R^- R^+ + 1 - T^2) \pm \sqrt{(R^- R^+ + 1 - T^2)^2 - 4R^- R^+}}{2R^-}, \\ e^{-i\omega\sigma d} &= \frac{T}{R^+ r^- + 1} = \frac{T}{R^- r^+ + 1} = \frac{2R^-}{R^+ + r^+} = \frac{R^- + r^-}{Tr^+}. \end{aligned} \quad (\text{F.4})$$

The sign of the first two equations are chosen to satisfy the passivity condition and χ_e , ρ_e , and K_e are subsequently evaluated. These equations are slightly different from those given in [9] and extend the method proposed in [41, 42], which was already used in [43].

Appendix G. Direct numerical calculation of the effective properties from the total transfer matrix

Once the total transfer matrix \mathbf{T} is calculated, it is directly assimilated to $\exp \mathbf{A}_e^{num} d$. From Eq. (F.1), it is clear that the eigenvectors of \mathbf{T} and \mathbf{A}_e^{num} are identical and that the exponential of the eigenvalues of $\mathbf{A}_e^{num} d$ are the eigenvalues of \mathbf{T} . Following the idea of [13], we immediately end up with

$$\mathbf{A}_e^{num} = \frac{1}{d} \mathbf{V} \text{diag} (\log (\Lambda^\pm)) \mathbf{V}^{-1}, \quad (\text{G.1})$$

where Λ^\pm are the eigenvalues of \mathbf{T} and \mathbf{V} the associated eigenvector matrix. The three quantities χ_e^{num} , ρ_e^{num} , and K_e^{num} are subsequently evaluated.

References

- [1] J.R. Willis. Variational principles for dynamic problems for inhomogeneous elastic media. *Wave Motion*, 3:1 – 11, 1981.
- [2] I. Lindell, A. Sihvola, S. Tretyakov, and A. J. Viitanen. *Electromagnetic waves in chiral and bi-isotropic media*, pages 1–22. Artech House, 1994.
- [3] A. Merkel, V. Romero-García, J.-P. Groby, J. Li, and J. Christensen. Unidirectional zero sonic reflection in passive \mathcal{PT} -symmetric willis media. *Phys. Rev. B*, 98:201102, 2018.
- [4] S. Koo, C. Cho, Jh Jeong, and N. Park. Acoustic omni meta-atom for decoupled access to all octants of a wave parameter space. *Nat Commun*, 7:13012, 2016.
- [5] J. Li, C. Shen, A. Díaz-Rubio, S. Tretyakov, and S. Cummer. Systematic design and experimental demonstration of bianisotropic metasurfaces for scattering-free manipulation of acoustic wavefronts. *Nat Commun*, 9:1342, 2018.
- [6] L. Quan, D. L. Sounas, and A. Alù. Nonreciprocal willis coupling in zero-index moving media. *Phys. Rev. Lett.*, 123:064301, 2019.
- [7] T. Frenzel, E. Köpflet, J. andJung, M. Kadic, and M. Wegener. Ultrasound experiments on acoustical activity in chiral mechanical metamaterials. *Nat Commun*, 10:3384, 2019.
- [8] Y. Zhai, H.-S. Kwon, and B.-I. Popa. Active willis metamaterials for ultracompact nonreciprocal linear acoustic devices. *Phys. Rev. B*, 99:220301, 2019.

- [9] M. B. Muhlestein, C. F. Sieck, P. S. Wilson, and M. R. Haberman. Experimental evidence of willis coupling in a one-dimensional effective material element. *Nat Commun*, 8:15625, 2017.
- [10] Y. Liu, Z. Liang, J. Zhu, L. Xia, O. Mondain-Monval, T. Brunet, A. Alù, and J. Li. Willis metamaterial on a structured beam. *Phys. Rev. X*, 9:011040, 2019.
- [11] C. F. Sieck, A. Alù, and M. R. Haberman. Origins of willis coupling and acoustic bianisotropy in acoustic metamaterials through source-driven homogenization. *Phys. Rev. B*, 96:104303, 2017.
- [12] M.-F. Ponge, Poncelet; O., and D. Torrent. Dynamic homogenization theory for nonlocal acoustic metamaterials. *Extreme Mechanics Letters*, 12:71 – 76, 2017.
- [13] A. L. Shuvalov, A. A. Kutsenko, A. N. Norris, and O. Poncelet. Effective willis constitutive equations for periodically stratified anisotropic elastic media. *Proc. R. Soc. A.*, 467:17491769, 2011.
- [14] S. Nemat-Nasser, J. R. Willis, A. Srivastava, and A. V. Amirkhizi. Homogenization of periodic elastic composites and locally resonant sonic materials. *Phys. Rev. B*, 83:104103, 2011.
- [15] A. Melnikov, Y. K. Chiang, Q. Li, S. Oberst, A. Alù, S. Marburg, and D. Powell. Acoustic meta-atom with experimentally verified maximum willis coupling. *Nat Commun*, 10:3148, 2019.
- [16] N. Jiménez, V. Romero-García, Pagnuex V., and J.-P. Groby. Rainbow-trapping absorbers: Broadband, perfect and asymmetric sound absorption by subwavelength panels with transmission. *Sci. Rep.*, 7:13595, 2017.
- [17] C. Shen, J. Li, X. Peng, and S. A. Cummer. Synthetic exceptional points and unidirectional zero reflection in non-hermitian acoustic systems. *Phys. Rev. Materials*, 2:125203, 2018.
- [18] Y. Aurégan and V. Pagneux. \mathcal{PT} -symmetric scattering in flow duct acoustics. *Phys. Rev. Lett.*, 118:174301, 2017.
- [19] Y. M. Seo, J. J. Park, S. H. Lee, C. M. Park, C. K. Kim, and S. H. Lee. Acoustic metamaterial exhibiting four different sign combinations of density and modulus. *J. Appl. Phys.*, 111, 2012.
- [20] S. H. Lee, C. M. Park, Y. M. Seo, Z. G. Wang, and C. K. Kim. Composite acoustic medium with simultaneously negative density and modulus. *Phys. Rev. Lett.*, 104:054301, 2010.
- [21] F. Zangeneh-Nejad and R. Fleury. Active times for acoustic metamaterials. *Reviews in Physics*, 4:100031, 2019.
- [22] A. Nemat-Nasser and A. Srivastava. Overall dynamic constitutive relations of layered elastic composites. *J. Mech. Phys. Solids*, 59:1953 – 1965, 2011.
- [23] C. Moler and C Van Loan. Nineteen dubious ways to compute the exponential of a matrix, twenty-five years later. *SIAM Rev.*, 45:349, 2003.
- [24] T Feng, Fu Liu, W. Yim Tam, and J. Li. Effective parameters retrieval for complex metamaterials with low symmetries. *EPL*, 102:18003, 2013.
- [25] J. L. Auriault and G. Bonnet. Dynamique des composites élastiques périodiques. *Arch. Mech.*, 37:269–284, 1985.
- [26] Z. Liu, X. Zhang, Y. Mao, Y. Y. Zhu, Z. Yang, C. T. Chan, and P. Sheng. Locally resonant sonic materials. *Science*, 289:1734–1736, 2000.
- [27] N. Fang, D. Xi, J. Xu, M. Ambati, W. Srituravanich, C. Sun, and X. Zhang. Ultrasonic metamaterials with negative modulus. *Nature Mater*, 5:452–456, 2005.
- [28] Z. Yang, J. Mei, M. Yang, N. H. Chan, and P. Sheng. Membrane-type acoustic metamaterial with negative dynamic mass. *Phys. Rev. Lett.*, 101:204301, 2008.
- [29] J. Li and C. T. Chan. Double-negative acoustic metamaterial. *Phys. Rev. E*, 70:055602, 2004.
- [30] M. Niskanen, J.-P. Groby, A. Duclos, O. Dazel, J. C. Le Roux, N. Poulain, T. Huttunen, and T. Lhivaara. Deterministic and statistical characterization of rigid frame porous materials from impedance tube measurements. *J. Acoust. Soc. Am.*, 142:2407–2418, 2017.
- [31] M. Malléjac, A. Merkel, J. Sánchez-Dehesa, J. Christensen, V. Tournat, J.-P. Groby, and V. Romero-García. Zero-phase propagation in realistic plate-type acoustic metamaterials. *Appl. Phys. Lett.*, 115:134101, 2019.
- [32] V. Romero-García, G. Theocharis, O. Richoux, A. Merkel, V. Tournat, and V. Pagneux. Perfect and broadband acoustic absorption by critically coupled sub-wavelength resonators. *Sci. Rep.*,

- 6:19519, 2016.
- [33] W. Huang, L. Schwan, V. Romero-García, J.-M. Génevaux, and J.-P. Groby. 3d-printed sound absorbing metafluid inspired by cereal straws. *Sci. Rep.*, 9:8496, 2019.
 - [34] G. Maugin. *Non-Classical Continuum Mechanics - A Dictionary*. Advanced Structured Materials. Springer, Singapore, 2017.
 - [35] C. Lagarrigue, J. P. Groby, V. Tournat, O. Dazel, and O. Umnova. Absorption of sound by porous layers with embedded periodic arrays of resonant inclusions. *J. Acoust. Soc. Am.*, 134:4670–4680, 2013.
 - [36] L. Schwan, O. Umnova, C. Boutin, and J.-P. Groby. Nonlocal boundary conditions for corrugated acoustic metasurface with strong near-field interactions. *J. Appl. Phys.*, 123:091712, 2018.
 - [37] J. Pierre, B. Dollet, and V. Leroy. Resonant acoustic propagation and negative density in liquid foams. *Phys. Rev. Lett.*, 112:148307, 2014.
 - [38] A. Merkel, G. Theocharis, O. Richoux, V. Romero-Garca, and V. Pagneux. Control of acoustic absorption in one-dimensional scattering by resonant scatterers. *Appl. Phys. Lett.*, 107:244102, 2015.
 - [39] F. Bongard, H. Lissek, and J. R. Mosig. Acoustic transmission line metamaterial with negative/zero/positive refractive index. *Phys. Rev. B*, 82:094306, 2010.
 - [40] M. R. Stinson. The propagation of plane sound waves in narrow and wide circular tubes, and generalization to uniform tubes of arbitrary crosssectional shape. *J. Acoust. Soc. Am.*, 89:550–558, 1991.
 - [41] A. M. Nicolson and G. F. Ross. Measurement of the intrinsic properties of materials by time-domain techniques. *IEEE Trans. Instrum. Meas.*, 19:377–382, 1970.
 - [42] W. B. Weir. Automatic measurement of complex dielectric constant and permeability at microwave frequencies. *Proc. IEEE*, 62:33–36, 1974.
 - [43] V. Fokin, M. Ambati, C. Sun, and X. Zhang. Method for retrieving effective properties of locally resonant acoustic metamaterials. *Phys. Rev. B*, 76:144302, 2007.